



UNIVERSITY OF LEEDS

This is a repository copy of *Structural basis of N-Myc binding by Aurora-A and its destabilization by kinase inhibitors*.

White Rose Research Online URL for this paper:
<http://eprints.whiterose.ac.uk/105919/>

Version: Accepted Version

Article:

Richards, MW orcid.org/0000-0003-1108-2825, Burgess, S
orcid.org/0000-0003-0361-0691, Poon, E et al. (4 more authors) (2016) Structural basis of N-Myc binding by Aurora-A and its destabilization by kinase inhibitors. *Proceedings of the National Academy of Sciences*, 113 (48). pp. 13726-13731. ISSN 0027-8424

<https://doi.org/10.1073/pnas.1610626113>

© 2016, National Academy of Sciences. This is an author produced version of a paper published in *Proceedings of the National Academy of Sciences*. Uploaded in accordance with the publisher's self-archiving policy.

Reuse

Items deposited in White Rose Research Online are protected by copyright, with all rights reserved unless indicated otherwise. They may be downloaded and/or printed for private study, or other acts as permitted by national copyright laws. The publisher or other rights holders may allow further reproduction and re-use of the full text version. This is indicated by the licence information on the White Rose Research Online record for the item.

Takedown

If you consider content in White Rose Research Online to be in breach of UK law, please notify us by emailing eprints@whiterose.ac.uk including the URL of the record and the reason for the withdrawal request.



eprints@whiterose.ac.uk
<https://eprints.whiterose.ac.uk/>

Structural basis of N-Myc binding by Aurora-A and its destabilization by kinase inhibitors

Mark W. Richards ^a, Selena G. Burgess ^a, Evon Poon ^b, Anne Carstensen ^c,
Martin Eilers ^c, Louis Chesler ^b, Richard Bayliss ^{a,d*}

- a. Astbury Centre for Structural and Molecular Biology, Faculty of Biological Sciences, and Cancer Research UK Leeds Centre, University of Leeds, Leeds LS2 9JT, UK
- b. Division of Clinical Studies and Cancer Therapeutics, The Institute of Cancer Research, The Royal Marsden NHS Trust, 15 Cotswold Rd, Belmont, Sutton, Surrey SM2 5NG, UK
- c. Theodor Boveri Institute and Comprehensive Cancer Center Mainfranken, Biocenter, University of Würzburg, Am Hubland, 97074 Würzburg, Germany
- d. Department of Cancer Studies, University of Leicester, Leicester LE1 9HN, UK

* Correspondence should be addressed to R.B. (r.w.bayliss@leeds.ac.uk)

Classification: Biological Sciences; Biochemistry
Keywords: Structural Biology, Aurora-A kinase, N-Myc, Neuroblastoma
Data deposition: The atomic coordinates and structure factors have been deposited in the Protein Data Bank www.pdb.org with PDB code **5G1X**.

The authors declare no conflict of interest.

Abstract

Myc family proteins promote cancer by inducing widespread changes in gene expression. Their rapid turn-over by the ubiquitin-proteasome pathway is regulated through phosphorylation of Myc Box I and ubiquitination by SCF^{Fbxw7}. However, N-Myc protein is stabilized in neuroblastoma by Aurora-A kinase in a manner that is sensitive to certain Aurora-A-selective inhibitors. Here we identify a direct interaction between the catalytic domain of Aurora-A and a site flanking Myc Box I that also binds SCF^{Fbxw7}. We determine the crystal structure of the complex between Aurora-A and this region of N-Myc to 1.72 Å resolution. The structure indicates that the conformation of Aurora-A induced by compounds such as alisertib and CD532 is not compatible with binding of N-Myc, explaining the activity of these compounds in neuroblastoma cells and providing a rational basis for the design of cancer therapeutics optimized for destabilization of the complex. We also propose a model for the stabilization mechanism in which binding to Aurora-A alters how N-Myc interacts with SCF^{Fbxw7} to disfavor the generation of Lys48-linked poly-Ub chains.

Significance

Elevated levels of N-Myc protein drives cancers such as neuroblastoma. Accumulation of N-Myc in these cancer cells depends upon the formation of a complex with Aurora-A kinase in which the N-Myc is not properly degraded. We mapped the region of N-Myc that interacts with Aurora-A and determined the molecular structure of the complex. Since this region also interacts with cellular machinery that targets N-Myc for degradation, we also seek to provide insights into the mechanism of stabilization of N-Myc by Aurora-A. The structure also explains how compounds that induce distorted conformations of Aurora-A are able to disrupt the interaction with N-Myc and may provide a basis for designing better compounds that work in this way for treatment of neuroblastoma.

/body

Introduction

Myc proteins are transcription factors that markedly alter gene expression through both activation and repression of transcription (1, 2). Three Myc protein family members can be aberrantly expressed in human cancers. c-Myc (Myc) was first discovered as the cellular homologue of the viral v-Myc oncoprotein and is frequently deregulated in a wide range of human cancers (3-5). N-Myc (MYCN) and L-Myc (MYCL) were subsequently identified as the products of amplified genes in neuroblastoma and small cell lung cancer, respectively (6-8). Inhibition of Myc is a validated therapeutic strategy, but efforts to develop clinical compounds that target Myc proteins directly have failed (9).

c-Myc, N-Myc and L-Myc have regions of sequence homology that mediate interactions with critical partner proteins such as Max, WDR5, TRRAP, PAF1C and Aurora-A (10). The most C-terminal of these regions forms an essential DNA-binding domain through formation of a basic helix-loop-helix leucine zipper domain in complex with Max (9, 11). Other conserved sequence motifs called Myc boxes (MB0-IV) serve as docking sites for protein-protein interactions (10, 12, 13). The Myc transactivation domain (TAD), spans the N-terminal conserved motifs MB0, MB1 and MBII. The TAD of c-Myc is intrinsically disordered, as reported by circular dichroism and nuclear magnetic resonance spectroscopy, but there are transient secondary structure elements that, in some cases, become stable in complex with binding partners (12, 14, 15).

The stability of Myc proteins is regulated by phosphorylation within MB1, which targets the protein for ubiquitylation and proteolysis. For example, N-Myc is first phosphorylated on Ser62 by Cdk1/cyclin B, then phosphorylated on Thr58 by Gsk3 β (16). Dephosphorylation of Ser62 by PP2A directs the activity of the E3 ubiquitin ligase SCF^{Fbxw7} to modify N-Myc with K48-linked ubiquitin chains (17, 18). In neuroblastoma cells, the Ser/Thr protein kinase Aurora-A blocks this process, resulting in an excess of N-Myc protein (19). Aurora-A binds to the N-Myc/SCF^{Fbxw7} complex, and reduces the proportion of K48 linkages in the poly-ubiquitin chains. Catalytic activity of Aurora-A is not required for N-Myc stabilization, and the underlying mechanism is unclear. Some Aurora-A inhibitors such as MLN8237/alisertib and CD532 can destabilize N-Myc by disrupting the complex, whilst other Aurora-A inhibitors have no effect (19, 20). The current hypothesis is

that the destabilizing inhibitors alter the conformation of Aurora-A in ways that disrupt the complex, whereas inhibitors that compete with ATP without causing a conformational change leave the complex intact (20-22).

We set out to investigate the structural basis of Aurora-A stabilization of N-Myc and the effect of Aurora-A inhibitors on the complex. Here we show that the catalytic domain of Aurora-A interacts directly with N-Myc through binding sites that flank either side of MBI. We present a crystal structure of the complex between Aurora-A and a fragment of N-Myc corresponding to the region immediately C-terminal to MBI which reveals Aurora-A in a fully active conformation that is incompatible with inhibitors of Aurora-A that disrupt the complex. Biochemical studies show an interaction between SCF^{Fbxw7} and the same region of N-Myc and we propose that the way in which Aurora-A interferes with this interaction changes N-Myc ubiquitination to promote stability.

Results and Discussion

Structural basis of the interaction between N-Myc and Aurora-A. To show that Aurora-A and N-Myc interact directly, we carried out a co-precipitation experiment using a GST-Aurora-A kinase domain fusion protein incubated with a range of purified fragments from the N-Myc TAD (Fig. S1A). This method identified residues 28-89 of N-Myc as the minimal Aurora-A-interaction region (AIR), which spans from MB0, through MBI but does not include MBII or beyond (Fig. 1A). The binding affinity of Aurora-A for the AIR was quantified as $2.9 \mu\text{M} \pm 0.5$ by ELISA (Fig. S1B) and $1.0 \mu\text{M} \pm 0.3$ by competition AlphaScreen™ assay (Fig. 1B). The presence of a tryptophan residue towards the C-terminus of this N-Myc fragment was striking, and mutation of Trp88 to alanine abrogated the interaction in the context of the entire N-Myc TAD fragment (residues 1-137) in a precipitation experiment with GST-tagged Aurora-A catalytic domain (residues 122-403); the TAD of N-Myc did not interact with GST alone and, together, these results indicate that the interaction is specific (Fig. S1C).

To elucidate the structural basis of the Aurora-A/N-Myc interaction, we crystallized a complex between the Aurora-A kinase domain, with surface cysteines mutated to enhance stability (Aurora-A^{C290A/C393A}), with a synthetic N-Myc peptide corresponding to residues 28-89. The crystals yielded diffraction data to 1.72 Å resolution and we solved the structure by molecular replacement using an existing

structure of Aurora-A^{C290A/C393A} (Table S1 and Fig. S1D). Residues 28-60 of N-Myc are not observed in the structure while residues 61-89 are associated with the cleft between the N- and C- lobes of the Aurora-A kinase domain formed by the α B/ α C helices, activation loop and α G helix (Fig. 1C). N-Myc residues 76-89 form an α -helix, which packs onto the C-lobe of Aurora-A at a surface formed by Tyr334, Gln335 and Tyr338 with its N-terminus pointing towards the substrate-binding region. Both ends of the α -helix are capped by tryptophan residues (Trp77 and Trp88) whose sidechains pack against the surface of Aurora-A. Key intermolecular interactions include a salt-bridge between Glu73 of N-Myc and Lys143 from the Gly-rich loop on the N-lobe of Aurora-A, a further interaction between Gln335 of Aurora-A and Trp88 of N-Myc and the insertion of the Trp77 sidechain of N-Myc into the hydrophobic P+1 pocket in the activation loop region of Aurora-A (Fig. 1D). A pair of prolines (P74 and P75) break the α -helix at its N-terminus and directs the chain towards the Aurora-A N-lobe. Residues 69-71 are hydrogen-bonded into a turn and residues 61-67 are bound into a groove between the N-lobe and the surface formed by the activation loop.

The region of N-Myc observed in the crystal structure starts at the C-terminus of MBI, and is not conserved in c-Myc (Fig. S2A). Our initial mapping suggested that this region was insufficient for binding, so we used a more sensitive assay, based on changes in fluorescence polarization (FP) using synthetic peptides of N-Myc, to confirm that residues 61-89 of N-Myc bind Aurora-A independently, with a measured K_d of 12 μ M (Fig. S2B). N-Myc peptides with E73K or W77A mutations reduced binding to Aurora-A, consistent with their observed contributions to the interface in the crystal structure (Fig. S2B). Similarly, the contributions of Aurora-A Y334 and Q335 to the interaction were confirmed.

The section of the AIR that was not resolved in the crystal structure, residues 28-60 of N-Myc, includes the MB0 and MBI regions and is conserved in c-Myc (Fig. S2A). Having shown that the C-terminal part of the AIR was able to bind Aurora-A independently, we looked for further sub-fragments that might contribute to binding with a sensitive pull-down assay using peptides spanning the region, under less stringent conditions than the first set of pull-downs used for mapping the interaction (Fig. S2C). In addition to residues 61-89, a region corresponding to MB0 was also capable of independent interaction with Aurora-A. Using the FP assay, we confirmed that a peptide spanning residues 19-47 of N-Myc, including MB0, binds independently to Aurora-A (Fig. S2D). The presence of conserved aromatic residues in this region is striking (F28, Y29, F35, Y36), and these were shown to contribute to

the interaction with Aurora-A (Fig. S2D). In contrast to the established roles of the regions flanking it, MBI itself does not appear to contribute to the interaction with Aurora-A because a peptide corresponding to residues 44-64 showed no binding in the peptide co-precipitation assay (Fig. S2C). Consistent with this, neither the phosphorylation status of the phosphodegron residues Thr58 and Ser62, nor mutation of residues 52-56 to alanine, affected Aurora-A binding of the N-Myc 28-89 peptide (Fig. S2E). We postulate that the flanking regions either side of MBI form specific interactions with Aurora-A, linked by the MBI region itself, which interacts in a phosphorylation-dependent manner with FbxW7, but makes no critical interactions with Aurora-A.

The interaction of N-Myc activates Aurora-A and competes with TPX2. When bound to N-Myc, Aurora-A is in a fully active conformation, similar to that observed for the Aurora-A/TPX2 complex (Fig. 2A) (23). TPX2 binds to Aurora-A through its first 43 residues: aa7-21 at a site on the N-lobe and aa30-43 at a site between the two lobes. The conformation adopted by Aurora-A when bound to TPX2 is incompatible with the interaction of N-Myc residues 61-67 (Fig. 2B). Most clearly, there is a steric clash because Leu61 of N-Myc binds to the same pocket on the Aurora-A surface as Trp34/Phe35 of TPX2. To accommodate the marked increase in size in going from the single Leu side chain of N-Myc to the two bulky side chains of TPX2, the side chain of Aurora-A residue His187 rotates out of the pocket in the TPX2-bound conformation. Side chains on the α C-helix of Aurora-A such as His176 and Arg179, are also observed in different positions, suggesting that the N-terminal stretch of TPX2 (Tyr8/Tyr10) that binds on one side of the α C-helix is incompatible with binding of N-Myc to the other side of the α C-helix. Consistent with this structural analysis, the first 43 amino acids of TPX2 and the AIR of N-Myc compete for binding to Aurora-A (Fig 2C) and they also have comparable affinities, since K_d values of 2-3 μ M were measured for both proteins in ELISA assays using immobilized Aurora-A (Fig. S1B). Competition with TPX2 was observed for the individual regions of the AIR both N- and C- terminal to MB1 (Fig. 2C) suggesting that the binding site for MB0 on Aurora-A also overlaps with that of TPX2. The AIR of N-Myc, like TPX2, activates initially unphosphorylated Aurora-A, and so there is also functional overlap between these two Aurora-A binding proteins (Fig. 2D, Fig. S3). The crystal structure reported here does not reveal the mechanism by which N-Myc activates Aurora-A because residues 61-89 of N-Myc were not sufficient to activate Aurora-A, and we used Aurora-A pre-phosphorylated on Thr288 to form the complex. However, it is clear that N-Myc, like TPX2, is able to trigger Aurora-A activation through protein-

protein interactions, and the result is a stabilized conformation of Aurora-A in which the activation loop forms a platform for the binding of N-Myc residues 61-89 (Fig. 2E). Furthermore, as shown in Fig. S3, Aurora-A is able to efficiently phosphorylate residues within the 28-89 region of N-Myc *in vitro*.

The conformation of Aurora-A bound to N-Myc is incompatible with inhibitors that destabilize the interaction. Previous studies showed that ATP-competitive inhibitors of Aurora-A such as MLN8054, MLN8237 and CD532 disrupt Aurora-A/N-Myc complex formation, resulting in destabilization of N-Myc in cell models. Crystal structures of Aurora-A in complex with MLN8054 or CD532 show distorted conformations of the kinase, notably in the positions of the activation loop and Gly-rich loop (20, 21). In contrast, most Aurora-A inhibitors, such as CCT137690, do not substantially affect the structure of the protein (24). There is no available crystal structure of MLN8237 bound to Aurora-A, but the chemical structures of MLN8054 and MLN8237 are almost identical and it is likely that MLN8237 induces a similar conformation in Aurora-A. We compared the structures of Aurora-A in complex with N-Myc, MLN8054, CD532 and CCT137690 (Fig. 3A). Aurora-A grips N-Myc through interactions involving both N- and C-lobes of the kinase (colored orange in Fig. 3A). Binding of CCT137690 does not affect the relative orientation of the two kinase lobes. The activation loop of Aurora-A is disordered in the Aurora-A/CCT137690 structure because it is neither phosphorylated nor stabilized by a protein such as TPX2 or N-Myc, and there is no obvious mechanism by which CCT137690 could affect the activation loop. However, when bound to MLN8054 or CD532, the surfaces that form the binding site for residues 61-89 of N-Myc are moved apart through motions that twist the two kinase lobes relative to one another and displace the activation loop (Fig. 3B). The rearrangement of this binding site provides a possible mechanism by which compounds like MLN8054 disrupt the Aurora-A/N-Myc complex by acting as a 'wedge' that forces the kinase into an inactive conformation. The key differences between CCT137690 and MLN8054 are that only the latter makes a specific contact with the displaced activation loop and, while both compounds contact both the hinge and the Gly-rich loop, the 'wedge' effect is a function of the three-dimensional shape of MLN8054 in contrast to the flatter scaffold of CCT137690.

Consistent with the structural analysis, MLN8054 but not CCT137690 disrupted the direct interaction of the catalytic domain of Aurora-A with its binding sites within the AIR (Fig. 3C). Indeed, Aurora-A bound to MLN8054 displayed 2-3-fold reduced affinity for both of the binding sites within the AIR of N-Myc compared to

Aurora-A alone Fig. S4). Next, we used proximity ligation assays to quantify complex formation between endogenous N-Myc and Aurora-A proteins in a neuroblastoma cell-line (Fig. 3D,E) and observed significantly fewer interactions in cells treated with MLN8054 or MLN8237 than in untreated cells while the number of interactions was unaffected by treatment with CCT137690.

A model for the regulation of N-Myc ubiquitination by Aurora-A. In this study, we showed that Aurora-A binds N-Myc irrespective of its phosphorylation state, and interacts with regions of N-Myc that flank MBI. The binding interaction between the Aurora-A catalytic domain and N-Myc residues 61-89 that we have resolved is immediately adjacent to the phospho-degron motif centered on Thr58, phosphorylation of which is required for recognition of N-Myc by SCF^{FbxW7}. Thus, binding of Aurora-A might affect the interaction of N-Myc with SCF^{FbxW7}. Using purified proteins, we discovered that SCF^{FbxW7}, like Aurora-A, interacts with N-Myc irrespective of the phosphorylation state of Thr58/Ser62 (Fig. 4A). Binding of SCF^{FbxW7} to N-Myc that is phosphorylated on Thr58/Ser62 was not affected by Aurora-A, consistent with non-overlapping binding sites on N-Myc. In contrast, the binding of SCF^{FbxW7} to unphosphorylated N-Myc was competed by Aurora-A. This observation suggested that the interaction of SCF^{FbxW7} with unphosphorylated N-Myc might depend on a binding site that overlaps with one or both of the Aurora-A binding sites that flank MBI. Binding of SCF^{FbxW7} was mapped to residues 61-89 of N-Myc and binding was also observed to residues 48-89 of N-Myc, but an unphosphorylated MBI peptide (residues 44-64) did not bind (Fig. 4B). Aurora-A efficiently competed with SCF^{FbxW7} for binding to residues 48-89 of N-Myc, in a dose-dependent manner, whereas a control protein (bovine serum albumin) did not compete (Fig. 4C). Taken together, these results show that there is competition between Aurora-A and SCF^{FbxW7} for binding to residues 61-89 of N-Myc, the region bound to Aurora-A in the crystal structure.

These observations suggest a working model by which Aurora-A could stabilize N-Myc through altering its interaction with SCF^{FbxW7}, which we put forward as a basis for further investigation (Fig. 4D). Recruitment of N-Myc to SCF^{FbxW7} is driven by the well-characterized interaction between the phospho-degron and FbxW7 that is regulated by phosphorylation of Thr58. However, a second interaction is also formed between N-Myc residues 61-89 and an unknown site on SCF^{FbxW7}. Aurora-A binds to N-Myc at sites that flank the phospho-degron, disrupting the interaction between residues 61-89 of N-Myc and SCF^{FbxW7}, but not the phospho-degron region, and so a

complex of Aurora-A, N-Myc and SCF^{Fbxw7} is formed. We postulate that the interaction between N-Myc residues 61-89 and SCF^{Fbxw7} is important for efficient polyubiquitination of N-Myc, and that disruption of this interaction by Aurora-A reduces the formation of Lys48-linked chains on N-Myc, as previously reported (19).

The dysregulation of Myc proteins is a feature of several cancers that are refractory to treatment and targeting Myc is a validated therapeutic strategy (9, 25-27). Unfortunately, there are currently no drug-like molecules that target Myc directly. Myc family proteins are intrinsically disordered proteins that dynamically adopt many conformations and, therefore, lack “druggable” pockets. This property has frustrated attempts to develop a drug-like molecule that directly targets the interaction of Myc with its binding partners. Here, we have characterized the complex with Aurora-A in which N-Myc is trapped in an ordered conformation. Disruption of the interaction can be achieved by targeting the ATP binding site of Aurora-A to induce a conformation that is incompatible with the binding of N-Myc, and early clinical trial data suggests these compounds may provide patient benefit when combined with chemotherapy (20, 22, 28). However, this approach would also target the main function of Aurora-A in the proper assembly and function of the mitotic spindle, and it is too early to know whether the potential benefit of this in targeting dividing cancer cells offsets the accompanying damage to normal tissue. Alternatively, it may be possible to inhibit the protein-protein interaction directly by targeting the interface. The structure of the Aurora-A/N-Myc complex provides a rational basis for the development of inhibitors that destabilize N-Myc and molecular coordinates of the interface that will facilitate structure-guided approaches to target the binding sites for ATP or N-Myc on Aurora-A.

Materials and Methods

Crystallography. Aurora-A 122-403 containing the mutations C290A and C393A was expressed and purified as described previously (29) and gel-filtrated into 20 mM Tris pH 7.5, 200 mM NaCl, 5 mM MgCl₂, 5 mM β-mercaptoethanol and 10% glycerol. An N-biotinyl peptide corresponding to residues 28-89 of N-Myc and carrying a phosphothreonine at position 58 (Peptide Synthetics) was dissolved to 10 mM in dimethylsulfoxide (DMSO). A mixture containing 300 μM Aurora-A, 5 mM adenosine diphosphate and 500 μM N-Myc peptide (with a final DMSO concentration of 5%) was incubated on ice for 1 h and then mixed 1:1 with reservoir solution (100 mM Bicine pH 9.0, 20% PEG 6000). Crystals were obtained by vapour diffusion at 18 °C

within a few days and were frozen in reservoir solution supplemented with 25% ethylene glycol. Diffraction data was collected from a single crystal at Diamond I03 and processed with *xia2* (30) (Table S1). The structure of the Aurora-A/N-Myc complex was solved by molecular replacement phasing using *Phaser* (31) with an existing Aurora-A structure (PDB 4CEG) (29) as the search model. Iterative modelling and refinement was carried out using *Coot* (32) and *phenix.refine* (33). Structure validation was carried out using Molprobity (34). Crystallographic data, refinement statistics and details of structure validation analysis are summarized in Table S1. Structure figures were prepared using PyMOL (<http://www.pymol.org>).

Co-precipitation assay. For *in vitro* peptide co-precipitation assays, 40 μ L of Streptactin Sepharose beads (IBA) were incubated with 900 μ L of 10 μ M N-biotinyl N-Myc peptides for 1 hour and then washed 3 times with pull-down buffer (50 mM Tris pH 7.5, 150 mM NaCl, 5 mM MgCl₂, 5 mM β -mercaptoethanol, 0.02% Tween-20). The beads were then incubated with 900 μ L of a solution containing analyte proteins, competing proteins or compounds as required, for 2 hours at 4 °C and then washed 3 times with 900 μ L pull-down buffer. Finally, the beads were eluted by boiling with 80 μ L SDS-loading buffer and the eluted proteins analysed by SDS-PAGE. Aurora-A 122-403 was used at a final concentration of 12 μ M. SCF^{FbxW7} incorporating GST-tagged FbxW7 (Millipore) was used at a final concentration of 5.5 ng/ μ L and visualised in precipitates by Western blotting using an anti-GST antibody (GE Healthcare).

Competition AlphaScreen™ assay. Biotinyl Avi-tagged Aurora-A 122-403 was produced as described previously (35). Appropriate concentrations of biotinyl Aurora-A 122-403 and 3xFlag-N-Myc 28-89 for use in competition experiments were determined in preliminary cross-titration experiments over a 0-300 nM range. The assay buffer was 50 mM Tris pH 7.5, 150 mM NaCl, 5 mM MgCl₂, 5 mM β -mercaptoethanol, 0.02% Tween-20 & 0.1% BSA. For competition assays, 10 nM biotinyl Aurora-A 122-403, 0.3 nM 3xFlag-N-Myc 28-89 and 0-160 μ M Aurora-A 122-403 were mixed together and incubated at room temperature (RT) for 1 hour in white, opaque 96-well $\frac{1}{2}$ area plates. 20 μ g/mL streptavidin donor beads and anti-Flag acceptor beads (PerkinElmer) were added simultaneously to each reaction under subdued lighting conditions and the plate incubated for a further 90 minutes. The signal from each reaction was read using an EnVision multilabel plate-reader (PerkinElmer). Data-points represent the mean of three experiments; error bars indicate SD. Data were analysed using Graphpad Prism 6 and the dependence of

the AlphaScreen™ signal on the concentration of competing Aurora-A 122-403 was fitted by non-linear regression to a one-site logIC50 equation where, under the selected reaction conditions, IC50 approximates K_d . Results are reported as $K_d \pm SE$.

***In situ* proximity ligation assay.** Kelly cells were cultured in RPMI 1640 supplemented with heat-inactivated fetal bovine serum. 500 nM compounds (as indicated) were added 4 hours prior to fixation. Cells were fixed with 4% paraformaldehyde for 30 minutes and permeabilized with phosphate buffered saline containing 0.2% Triton X-100 for a further 30 minutes. Cells were incubated with Duolink *In situ* blocking solution for 1 hour and then with antibodies against Aurora-A (Genetex) and N-Myc (Calbiochem) diluted into the same buffer for a further hour. *In situ* proximity ligation assays were carried out using the Duolink kit (Olink Bioscience) according to the manufacturers instructions. Images were collected and analysed using a Humphrey 730 field analyser system (Zeiss). The average number of interactions detected per cell was calculated and results are reported as the mean of three independent experiments $\pm SD$.

Kinase assay. ^{32}P -ATP kinase assays were performed as described with modifications as follows (36). Measurement of Aurora-A activity was carried out using reactions containing 0.625 μM dephosphorylated Aurora-A catalytic domain, 40 μM myelin basic protein (Sigma) and 0-50 μM N-Myc 28-89, N-Myc 61-89 or TPX2 1-43 peptides. Reactions were incubated at 21 °C for 45 minutes and total incorporation of ^{32}P radioisotope into Aurora-A, N-Myc 28-89 and myelin basic protein was then measured by scintillation counting. Results are the mean of two independent experiments $\pm SE$.

Acknowledgements

We thank the beamline scientists of Diamond I03 for assistance with data collection. This work was funded by grants from the European Research Council ("AuroMYC" to M.E. and R.B.), the Deutsche Krebshilfe (to M.E.), Cancer Research UK (Grant C24461/A12772 to R.B.).

Author contributions

M.W.R, S.G.B, E.P and A.C. carried out the experiments. M.W.R, S.G.B., E.P., M.E, L.C and R.B. designed the research. R.B. and M.W.R. wrote the manuscript.

References

1. Kress TR, Sabo A, & Amati B (2015) MYC: connecting selective transcriptional control to global RNA production. *Nat Rev Cancer* 15(10):593-607.
2. Wolf E, Lin CY, Eilers M, & Levens DL (2015) Taming of the beast: shaping Myc-dependent amplification. *Trends Cell Biol* 25(4):241-248.
3. Vennstrom B, Sheiness D, Zabielski J, & Bishop JM (1982) Isolation and characterization of c-myc, a cellular homolog of the oncogene (v-myc) of avian myelocytomatosis virus strain 29. *J Virol* 42(3):773-779.
4. Ciriello G, *et al.* (2013) Emerging landscape of oncogenic signatures across human cancers. *Nat Genet* 45(10):1127-1133.
5. Vogelstein B, *et al.* (2013) Cancer genome landscapes. *Science* 339(6127):1546-1558.
6. Kohl NE, *et al.* (1983) Transposition and amplification of oncogene-related sequences in human neuroblastomas. *Cell* 35(2 Pt 1):359-367.
7. Schwab M, *et al.* (1983) Amplified DNA with limited homology to myc cellular oncogene is shared by human neuroblastoma cell lines and a neuroblastoma tumour. *Nature* 305(5931):245-248.
8. Nau MM, *et al.* (1985) L-myc, a new myc-related gene amplified and expressed in human small cell lung cancer. *Nature* 318(6041):69-73.
9. Soucek L, *et al.* (2008) Modelling Myc inhibition as a cancer therapy. *Nature* 455(7213):679-683.
10. Tu WB, *et al.* (2015) Myc and its interactors take shape. *Biochim Biophys Acta* 1849(5):469-483.
11. Nair SK & Burley SK (2003) X-ray structures of Myc-Max and Mad-Max recognizing DNA. Molecular bases of regulation by proto-oncogenic transcription factors. *Cell* 112(2):193-205.
12. Helander S, *et al.* (2015) Pre-Anchoring of Pin1 to Unphosphorylated c-Myc in a Fuzzy Complex Regulates c-Myc Activity. *Structure* 23(12):2267-2279.
13. Jaenicke LA, *et al.* (2016) Ubiquitin-Dependent Turnover of MYC Antagonizes MYC/PAF1C Complex Accumulation to Drive Transcriptional Elongation. *Mol Cell* 61(1):54-67.
14. Fladvad M, *et al.* (2005) N and C-terminal sub-regions in the c-Myc transactivation region and their joint role in creating versatility in folding and binding. *J Mol Biol* 346(1):175-189.
15. Pineda-Lucena A, *et al.* (2005) A structure-based model of the c-Myc/Bin1 protein interaction shows alternative splicing of Bin1 and c-Myc phosphorylation are key binding determinants. *J Mol Biol* 351(1):182-194.
16. Sjostrom SK, Finn G, Hahn WC, Rowitch DH, & Kenney AM (2005) The Cdk1 complex plays a prime role in regulating N-myc phosphorylation and turnover in neural precursors. *Dev Cell* 9(3):327-338.

17. Welcker M, *et al.* (2004) The Fbw7 tumor suppressor regulates glycogen synthase kinase 3 phosphorylation-dependent c-Myc protein degradation. *Proc Natl Acad Sci U S A* 101(24):9085-9090.
18. Adhikary S & Eilers M (2005) Transcriptional regulation and transformation by Myc proteins. *Nat Rev Mol Cell Biol* 6(8):635-645.
19. Otto T, *et al.* (2009) Stabilization of N-Myc is a critical function of Aurora A in human neuroblastoma. *Cancer Cell* 15(1):67-78.
20. Gustafson WC, *et al.* (2014) Drugging MYCN through an allosteric transition in Aurora kinase A. *Cancer Cell* 26(3):414-427.
21. Dodson CA, *et al.* (2010) Crystal structure of an Aurora-A mutant that mimics Aurora-B bound to MLN8054: insights into selectivity and drug design. *Biochem J* 427(1):19-28.
22. Brockmann M, *et al.* (2013) Small molecule inhibitors of aurora-a induce proteasomal degradation of N-myc in childhood neuroblastoma. *Cancer Cell* 24(1):75-89.
23. Bayliss R, Sardon T, Vernos I, & Conti E (2003) Structural basis of Aurora-A activation by TPX2 at the mitotic spindle. *Mol Cell* 12(4):851-862.
24. Bavetsias V, *et al.* (2010) Imidazo[4,5-b]pyridine derivatives as inhibitors of Aurora kinases: lead optimization studies toward the identification of an orally bioavailable preclinical development candidate. *J Med Chem* 53(14):5213-5228.
25. Gustafson WC & Weiss WA (2010) Myc proteins as therapeutic targets. *Oncogene* 29(9):1249-1259.
26. Barone G, Anderson J, Pearson AD, Petrie K, & Chesler L (2013) New strategies in neuroblastoma: Therapeutic targeting of MYCN and ALK. *Clin Cancer Res* 19(21):5814-5821.
27. Hill RM, *et al.* (2015) Combined MYC and P53 defects emerge at medulloblastoma relapse and define rapidly progressive, therapeutically targetable disease. *Cancer Cell* 27(1):72-84.
28. DuBois SG, *et al.* (2016) Phase I Study of the Aurora A Kinase Inhibitor Alisertib in Combination With Irinotecan and Temozolomide for Patients With Relapsed or Refractory Neuroblastoma: A NANT (New Approaches to Neuroblastoma Therapy) Trial. *J Clin Oncol* 34(12):1368-1375.
29. Burgess SG & Bayliss R (2015) The structure of C290A:C393A Aurora A provides structural insights into kinase regulation. *Acta Crystallogr F Struct Biol Commun* 71(Pt 3):315-319.
30. Winter G, Lobley CM, & Prince SM (2013) Decision making in xia2. *Acta Crystallogr D Biol Crystallogr* 69(Pt 7):1260-1273.
31. McCoy AJ, *et al.* (2007) Phaser crystallographic software. *J Appl Crystallogr* 40(Pt 4):658-674.
32. Emsley P & Cowtan K (2004) Coot: model-building tools for molecular graphics. *Acta Crystallogr D Biol Crystallogr* 60(Pt 12 Pt 1):2126-2132.
33. Adams PD, *et al.* (2002) PHENIX: building new software for automated crystallographic structure determination. *Acta Crystallogr D Biol Crystallogr* 58(Pt 11):1948-1954.
34. Chen VB, *et al.* (2010) MolProbity: all-atom structure validation for macromolecular crystallography. *Acta Crystallogr D Biol Crystallogr* 66(Pt 1):12-21.

35. Burgess SG, *et al.* (2016) Allosteric inhibition of Aurora-A kinase by a synthetic vNAR domain. *Open Biology* 6:160089.
36. Burgess SG, *et al.* (2015) Aurora-A-Dependent Control of TACC3 Influences the Rate of Mitotic Spindle Assembly. *PLoS Genet* 11(7):e1005345.

Figure legends

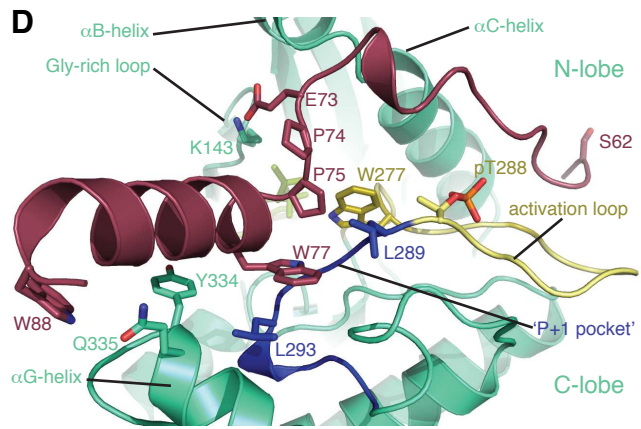
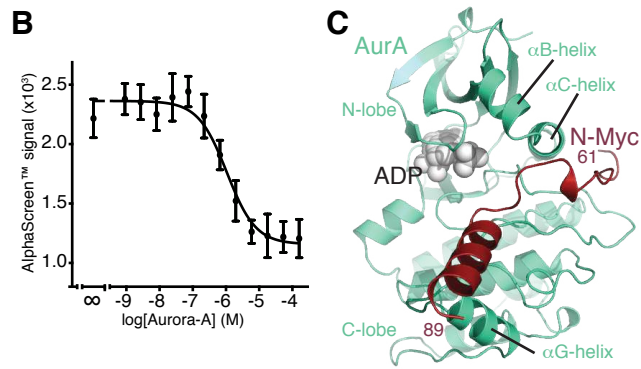
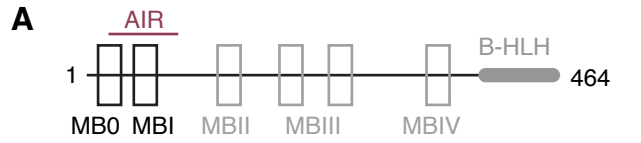
Fig. 1. Crystal structure of Aurora-A/N-Myc complex. (A) Domain structure of N-Myc with conserved regions indicated as boxes and the Aurora-A Interaction Region (AIR) marked with a red line. (B) Quantification of the binding affinity between Aurora-A kinase domain and the N-Myc AIR by competition AlphaScreen assay. Data represents the mean of three experiments \pm SD. (C) Crystal structure of Aurora-A^{C290A/C393A} catalytic domain (AurA, green cartoon) in complex with N-Myc residues 61-89 (N-Myc, red cartoon). (D) Magnified view of the structure with key residues shown as sticks.

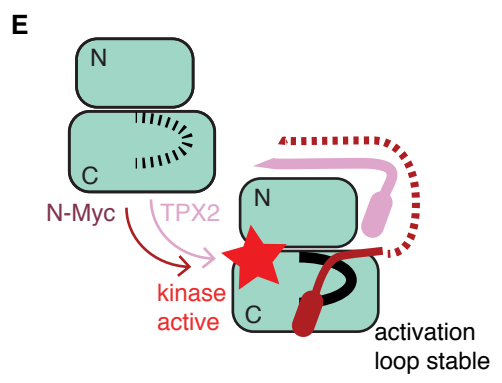
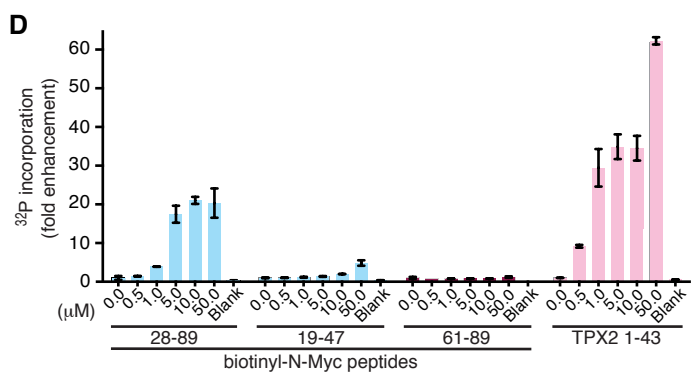
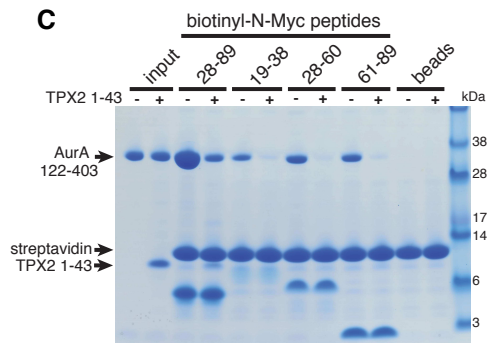
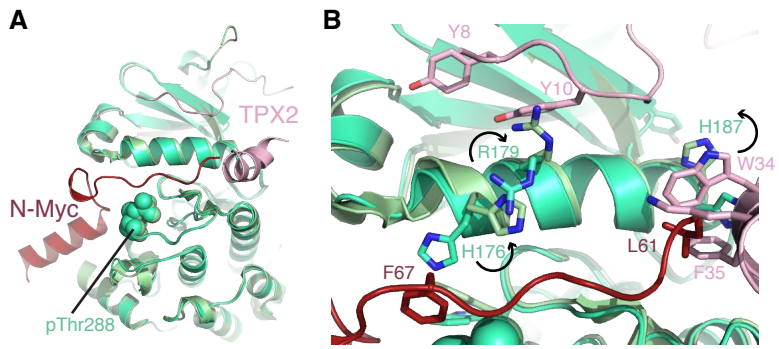
Fig. 2. Structural and functional comparison of Aurora-A interactions with N-Myc and TPX2. (A) Superposition of crystal structures of Aurora-A bound to N-Myc (colored red) and TPX2 (colored pink). Aurora-A bound to TPX2 is colored a lighter shade of green. (B) Magnified view of the superposed structures. The side-chain motions accompanying the transition from the N-Myc to the TPX2 complex are marked with black arrows. (C) Co-precipitation experiments to investigate competition between TPX2 (residues 1-43) and N-Myc fragments for binding to Aurora-A (residues 122-403), analysed by SDS-PAGE. The gel shows proteins co-precipitated with biotinyl-N-Myc peptides (as indicated) immobilized on streptavidin beads following incubation with 12 μ M Aurora-A catalytic domain in the presence or absence of a 5-fold molar excess of TPX2 1-43 protein. (D) Kinase assays to measure the activity of 0.625 μ M initially unphosphorylated Aurora-A catalytic domain in the presence of ³²P-ATP and varying concentrations N-Myc peptides (residues 28-89, 19-47 or 61-89) or TPX2 (residues 1-43), reported by scintillation counting. Data are the mean of two experiments \pm SE. (E) Schematic illustration of the activating interactions of N-Myc and TPX2 with Aurora-A. The unphosphorylated activation loop of Aurora-A is flexible (dashed black line) but becomes ordered upon kinase activation through binding of protein partners and autophosphorylation.

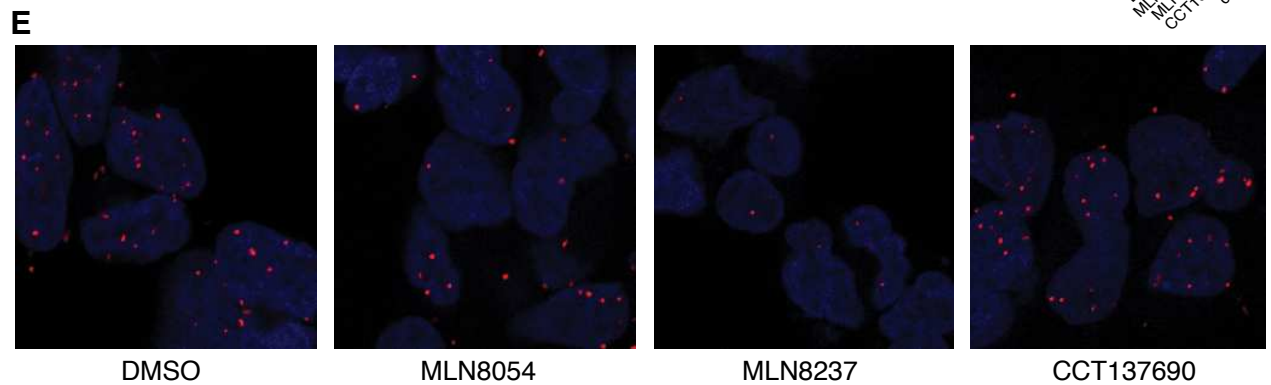
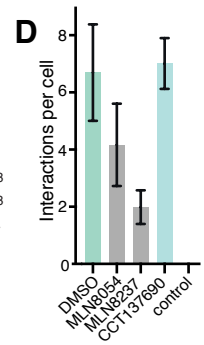
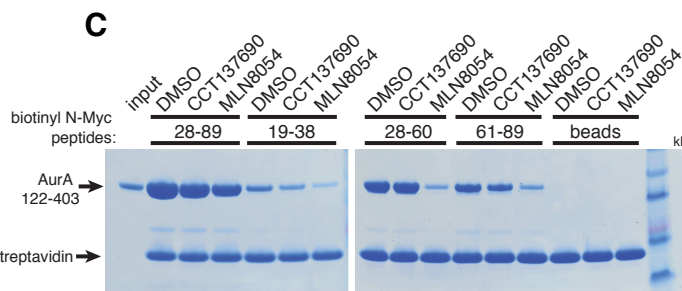
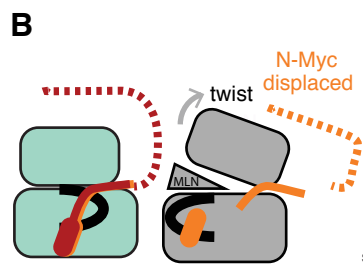
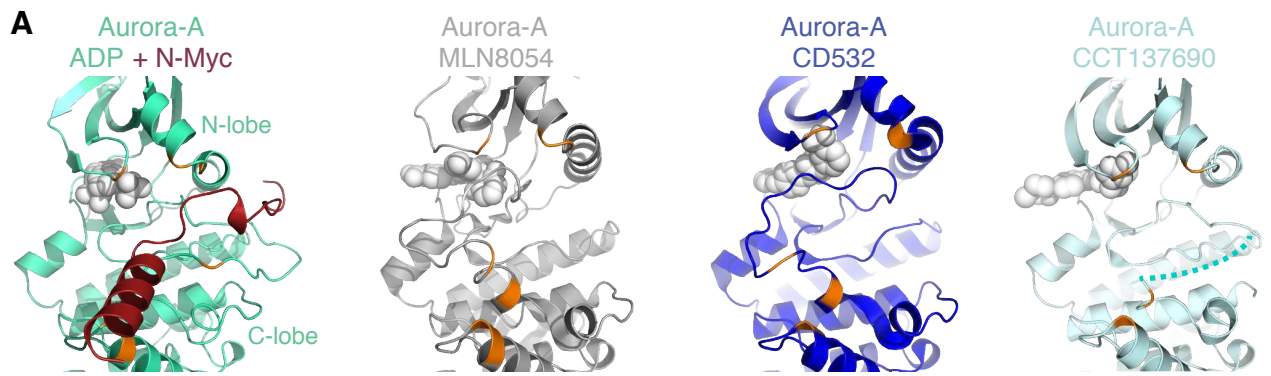
Fig. 3. The conformation of Aurora-A required for N-Myc binding is incompatible with the conformation induced by kinase inhibitors that disrupt the interaction. (A) Views of Aurora-A bound to N-Myc (PDB: 5G1X), MLN8054 (2WTV), CD532 (4J8M) and CCT137690 (2X6E). Key residues of Aurora-A (orange) that grasp N-Myc (dark red) remain in place in the presence of CCT137690 but are moved apart in the presence of MLN8054/8237 and even further apart in the presence of CD532. The dotted line in the rightmost panel indicates the disordered

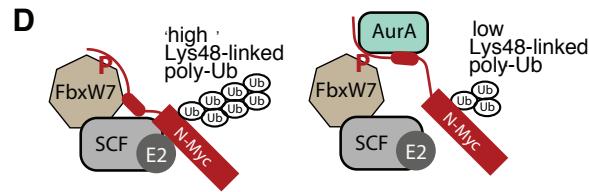
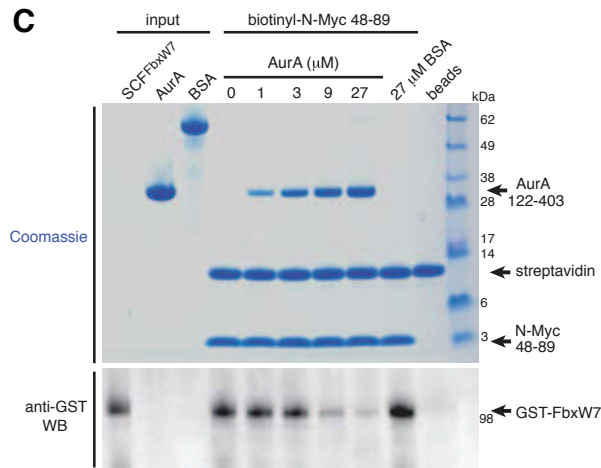
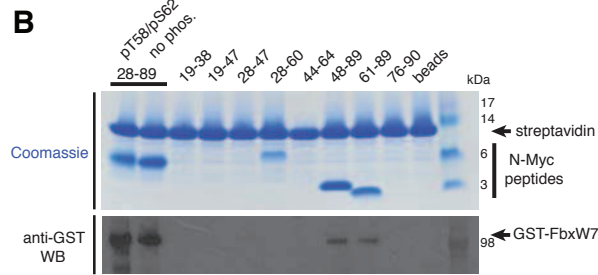
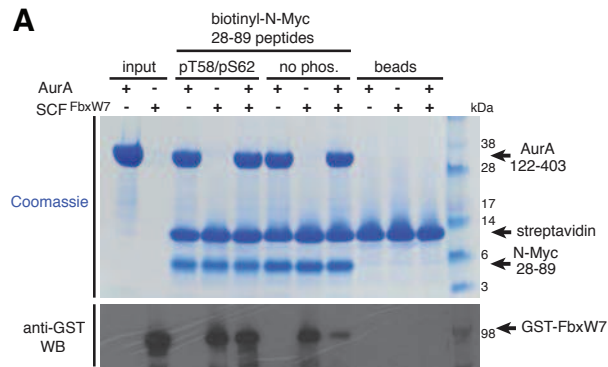
region of the activation loop. **(B)** Schematic model to explain the disruption of the N-Myc binding site by ATP-competitive inhibitors. The activation loop is shown in black. **(C)** Competition co-precipitation experiments using untagged Aurora-A catalytic domain and biotinylated N-Myc peptides immobilized on streptavidin beads in the presence of 20 μ M MLN8054 or CCT137690, using 0.2% DMSO as control. **(D)** Incidence of complex formation between N-Myc and Aurora-A observed *in situ* by proximity ligation assay in Kelly neuroblastoma cells treated with compounds as indicated. Data represents mean \pm SD. No antibodies were added to the control cells. **(E)** Representative images of Kelly cells used in D. Nuclei are indicated by DAPI staining (blue) and red foci indicate the position of Aurora-A/N-Myc complexes.

Fig. 4. Aurora-A alters the interaction of N-Myc with SCF^{FbxW7}. **(A)** Competition co-precipitation experiments using biotinylated N-Myc AIR peptides immobilized on streptavidin beads, incubated with 2 μ g SCF complex incorporating GST-tagged FbxW7 in the presence or absence of 12 μ M untagged Aurora-A catalytic domain. Binding of SCF^{FbxW7} to N-Myc was visualized by Western blot (WB) using anti-GST antibody. **(B)** Co-precipitation experiments using biotinylated N-Myc AIR fragment peptides immobilized on streptavidin beads and incubated with 2 μ g SCF complex incorporating GST-tagged FbxW7. Binding of SCF^{FbxW7} to N-Myc peptides was visualized by Western blot using an anti-GST antibody (lower panel). Equal loading of resin was assessed by Coomassie staining (upper panel). Note that, despite the uneven appearance of the peptides on the upper panel due to differences in migration and sensitivity to Coomassie staining, equal amounts were loaded into the experiments. **(C)** Co-precipitation experiments showing competition between SCF^{FbxW7} and Aurora-A for binding to N-Myc 48-89. Biotinylated N-Myc 48-89 peptide was immobilized on streptavidin beads and incubated with 2 μ g SCF^{FbxW7} complex in the presence of Aurora-A at a range of concentrations, or bovine serum albumin (BSA). FbxW7 co-precipitating with the peptide was visualized by anti-GST Western blot. **(D)** A working model to explain how the interaction between Aurora-A and N-Myc residues 61-89 may reduce ubiquitination to stabilize N-Myc. In this model, a low affinity interaction between the 61-89 region and SCF^{FbxW7} is required for N-Myc to be effectively modified with K48-linked polyubiquitin chains and competitive binding of Aurora-A to this region interferes with K48-linked polyubiquitination of N-Myc leading to reduced proteasomal degradation.









Supporting information

SI Methods

Protein production and co-precipitation assay. TPX2 1-43 and GST-Aurora-A 122-403 D274N were expressed and purified as described previously (Burgess et al., 2015). Constructs encoding 3xFlag-tagged fragments of the N-Myc transactivation domain and TPX-2 1-43 were expressed as His-NusA fusions in *Escherichia coli* BL21 (DE3) RIL cells and purified on 5 mL Chelating Sepharose columns (GE Healthcare) charged with nickel; the His-NusA tags were cleaved away using tobacco etch virus protease and removed by nickel affinity chromatography; the remaining 3xFlag-tagged polypeptides were further purified by anion exchange on a Resource Q column (GE Healthcare) over a 50-500 mM NaCl gradient in 20 mM Tris pH 7.5, 1 mM EDTA and then by gel filtration into TBS using a Superdex 75 column (GE Healthcare). 250 µg GST-Aurora-A 122-403 D274N or 100 µg of GST were immobilized on 40 µL of glutathione Sepharose beads (GE Healthcare) and incubated with 900 µL of 35 µM 3xFlag-N-Myc fragments (including compounds as required) for 2 hours in pull-down buffer. The beads were washed 4 times with 900 µL pull-down buffer. Bound proteins were analysed by SDS-PAGE and visualized by Coomassie staining and by anti-Flag immunoblotting (M2, Sigma).

ELISA assay. Pre-blocked HBC Streptavidin plates (Pierce) were incubated with 10 µg/mL biotinyl Avi-tagged-Aurora-A 122-403 for 30 minutes at RT. Wells were washed 3 times with 300 µL PBS supplemented with 0.1% Tween-20 (PBST). 0-40 µM 3xFlag-N-Myc 28-89 was added to the wells and incubated for 1 hour at RT. Negative control reactions containing no immobilised Aurora-A were also performed. Plates were washed with PBST followed by the addition 1:5000 of horse-radish peroxidase-conjugated anti-Flag antibody (abcam ab49763). Reactions were incubated at RT for a further 30 minutes and washed again with PBST. Binding of 3xFlag-N-Myc 28-89 was resolved by addition of 3,3',5,5'-Tetramethylbenzidine and the reaction quenched by the addition of 0.5 M H₂SO₄. Absorbance at 450 nm was read for each reaction. Data-points represent the mean of three experiments; error bars indicate SD. The data were fitted to a one-site specific binding equation by non-linear regression using Graphpad Prism 6. Results are reported as $K_d \pm SE$.

Fluorescence polarization assay. 50 nM fluorescein-labelled N-Myc aa61-89 or aa19-47 peptides (Pepceuticals) were incubated at 21 °C with Aurora-A kinase domain protein (aa122-403) at a range of concentrations in a buffer containing 25 mM HEPES pH 7.5, 150 mM NaCl, 5 mM MgCl₂, 5% glycerol, and 0.02% Tween-20 in a flat-bottomed, black 96-well plate at a total volume of 50 µl per sample. Dephosphorylated Aurora-A catalytic domain was made by co-expression with lambda phosphatase and purified in the same way as non-dephosphorylated protein (Burgess et al., 2015). To investigate the influence of MLN8054 on the interaction, the compound was dissolved in DMSO to a concentration of 10 mM and added to a final concentration of 600 µM to all samples; an equivalent quantity of DMSO (6%) was added to corresponding compound-free samples. Fluorescence polarization was measured using a Victor X5 instrument (PerkinElmer) at excitation and emission wavelengths of 480 nm and 535 nm. Data-points represent the mean of three experiments; error bars indicate SD. The dependence of fluorescence polarization upon Aurora-A concentration was fitted to a one-site total binding model by non-linear regression using GraphPad Prism 6. Results are reported as $K_d \pm SE$.

SI Figure Legends

Fig. S1. Interaction between N-Myc and Aurora-A. **(A)** Co-precipitation of fragments of the N-Myc transactivation domain with GST-Aurora-A kinase domain. Flag-tagged N-Myc fragments were incubated with GST-Aurora-A 122-403 D274N or GST alone immobilised on glutathione Sepharose beads. Co-precipitated N-Myc fragments were visualised by anti-Flag Western blot (WB). **(B)** Binding isotherms measured by ELISA quantifying the interaction of 3xFlag-N-Myc 28-89 (upper panel) and 3xFlag-N-Myc TPX2 1-43 (lower panel) with immobilised biotinyl Avi-tagged-Aurora-A 122-403. Data-points represent the mean of three experiments; error bars indicate SD. (Affinities of $2.9 \mu\text{M} \pm 0.5$ and 2.0 ± 0.3 were measured for 3xFlag-N-Myc 28-89 and 3xFlag-N-Myc TPX2 1-43 respectively.) **(C)** The specific interaction between GST-Aurora-A catalytic domain and Flag-tagged N-Myc TAD is abrogated by a single point mutation (Trp88). Glutathione resin precipitates were separated by SDS-PAGE followed by Western blot analysis and Coomassie Blue (CB) staining. **(D)** A representative region of the electron density map of the 1.72 Å crystal structure of the Aurora-A-N-Myc complex showing the interaction of tryptophan 77 of N-Myc (dark red) with a hydrophobic pocket on Aurora-A (pale green). The mesh represents a 2mFo-DFc map contoured at 1.0 σ .

Fig. S2. Verification of two binding sites for Aurora-A on N-Myc. (A) Sequence alignment of N-Myc and c-Myc in the Aurora-A interaction region. Asterisks, colons and full stops mark identical, conserved and conservatively substituted residues respectively. Conserved regions MB0 and MBI (incorporating the phospho-degron) are boxed and the two binding sites for Aurora-A within N-Myc, corresponding to the peptides used in B, are marked with dashed (19-47) and solid (61-89) red lines. **(B)** Binding isotherms measured by fluorescence polarization quantifying the interaction between Aurora-A catalytic domain and N-Myc residues 61-89. Data-points represent the mean of three experiments; error bars indicate SD. (Affinities of $12.1 \mu\text{M} \pm 0.6$ and $12.8 \mu\text{M} \pm 0.7$ were measured for binding of the phosphorylated and dephosphorylated Aurora-A respectively to wild-type peptide. N-Myc 61-89 peptides containing mutations E73K and W77A interacted with wild-type Aurora-A with affinities of $81.1 \mu\text{M} \pm 3.4$ and $106 \mu\text{M} \pm 4.5$, respectively. Measured affinities of Aurora-A mutants Y334A and Q335A for wild-type N-Myc 61-89 were $22.6 \mu\text{M} \pm 1.1$ and $16.1 \mu\text{M} \pm 0.8$, respectively.) **(C)** Co-precipitation experiments showing interaction of Aurora-A kinase domain with biotinyl-N-Myc peptides. (Note, some peptides do not stain with Coomassie.) **(D)** Binding isotherms measured by fluorescence polarization quantifying the interaction between Aurora-A catalytic domain and N-Myc residues 19-47. Data-points represent the mean of three experiments; error bars indicate SD. (Affinities of $11.1 \mu\text{M} \pm 0.4$ and $9.2 \mu\text{M} \pm 0.3$ were measured for the binding of the phosphorylated and dephosphorylated Aurora-A respectively to wild-type N-Myc 19-47 peptide. Affinities of $18.6 \mu\text{M} \pm 0.6$ and $23.7 \mu\text{M} \pm 0.8$ were measured for the binding of 19-47 peptides containing the mutations F28A and F35A respectively, while a peptide containing both of these mutations bound with a K_d of $114.0 \mu\text{M} \pm 4.0$. A Y29A, Y36A double mutant 19-47 peptide bound Aurora-A with a K_d of $68.8 \mu\text{M} \pm 2.3$.) **(E)** Co-precipitation experiments showing interaction of Aurora-A kinase domain with biotinyl-N-Myc 28-89 peptides carrying different phosphorylation marks within the region corresponding to the phospho-degron. 52-56_polyA, which is also included in the experiment, is a non-phosphorylated 28-89 peptide with residues 52-56 mutated to alanine. (The sequence of N-Myc in this region 51-KKFELLP-57 bears some resemblance to an Aurora-A consensus phosphorylation site (K/R/N-R-XS/T-B), with E54 in place of the P1 Ser/Thr. The 28-89 52-56_polyA peptide was used to investigate the possibility that a pseudosubstrate interaction between this region of N-Myc and Aurora-A might contribute to the binding.)

Fig. S3. Autoradiograph showing activation of Aurora-A by N-Myc 28-89 in the presence of ^{32}P -ATP. Initially unphosphorylated full-length Aurora-A shows enhanced autophosphorylation in the presence of N-Myc 28-89 peptide. The N-Myc peptide also becomes phosphorylated itself. Reactions contained 0.625 μM dephosphorylated full-length Aurora-A and 10 μM N-Myc 28-89. Samples were separated by SDS-PAGE and ^{32}P -incorporation into individual proteins visualised by autoradiography.

Fig. S4. Aurora-A ATP-competitive inhibitors and N-Myc interaction. Binding isotherms measured by fluorescence polarization quantifying the interaction of Aurora-A catalytic domain (red), and Aurora-A catalytic domain/MLN8054 complex (blue), with **(A)** N-Myc residues 19-47 and **(B)** N-Myc residues 61-89. Data-points represent the mean of three experiments; error bars indicate SD; binding affinities between Aurora-A and N-Myc peptides derived from curve-fitting are stated above as $K_d \pm \text{SE}$.

Table S1. Crystallographic data collection, refinement and structure validation statistics. Values in parentheses refer to the highest resolution shell.

	AurA/N-Myc complex
Lattice parameters	
Space group	$P3_2 2 1$
Cell dimensions	
<i>a</i> , <i>b</i> , <i>c</i> (Å)	86.52, 86.52, 92.21
α , β , γ	90.00, 90.00, 120.00
Data collection	
Resolution range (Å)	74.93-1.72 (1.76 –1.72) *
R_{merge} (%)	6.3 (74.3)
$I / \sigma I$	19.8 (3.4)
Completeness (%)	100 (100)
Redundancy	9.7 (9.7)
Refinement	
Resolution (Å)	74.3-1.72
No. reflections	42820
$R_{\text{work}} / R_{\text{free}}$	17.62 / 19.51
No. atoms	
Protein	2362
ADP/Mg ²⁺	29
Water	197
Mean <i>B</i> -factors	
Protein	28.09
ADP/Mg ²⁺	19.16
Water	37.17
Wilson <i>B</i> -factor	25.63
r.m.s. deviations	
bond lengths (Å)	0.005
bond angles (°)	1.043
MolProbity analysis	
All-atom clash-score	2.34
Rotamers outliers (%)	0
Ramachandran outliers (%)	0
Ramachandran favoured (%)	97.25
MolProbity score	1.15

